



# Local CFD kinetic model of cadmium vaporization during fluid bed incineration of municipal solid waste

J. Soria<sup>a,b</sup>, D. Gauthier<sup>b,\*</sup>, Q. Falcoz<sup>b</sup>, G. Flamant<sup>b</sup>, G. Mazza<sup>a</sup>

<sup>a</sup> Instituto Multidisciplinario de Investigación y Desarrollo de la Patagonia Norte (IDEPA, CONICET-UNCo) y Facultad de Ingeniería, Universidad Nacional del Comahue, Buenos Aires 1400, 8300 Neuquén, Argentina

<sup>b</sup> Laboratoire Procédés, Matériaux et Energie Solaire (CNRS-PROMES), 7 Rue du Four Solaire, Odeillo, 66120 Font-Romeu, France

## HIGHLIGHTS

- A 2-D local CFD model for simulating the Cd vaporization process is presented.
- It includes a kinetic expression of Cd vaporization into the incineration process.
- Pyrolysis, volatiles' combustion and residual carbon combustion are also taken into account.
- It fits very well the experimental results obtained on a lab-scale fluidized bed reported in literature.
- It also compares favorably with a model developed previously by the group.

## ARTICLE INFO

### Article history:

Received 31 July 2012

Received in revised form 7 January 2013

Accepted 8 January 2013

Available online xxx

### Keywords:

Heavy metal vaporization

Cadmium vaporization

Fluid bed waste incineration

Particle combustion

CFD model

## ABSTRACT

The emissions of heavy metals during incineration of Municipal Solid Waste (MSW) are a major issue to health and the environment. It is then necessary to well quantify these emissions in order to accomplish an adequate control and prevent the heavy metals from leaving the stacks. In this study the kinetic behavior of Cadmium during Fluidized Bed Incineration (FBI) of artificial MSW pellets, for bed temperatures ranging from 923 to 1073 K, was modeled. FLUENT 12.1.4 was used as the modeling framework for the simulations and implemented together with a complete set of user-defined functions (UDFs). The CFD model combines the combustion of a single solid waste particle with heavy metal (HM) vaporization from the burning particle, and it takes also into account both pyrolysis and volatiles' combustion. A kinetic rate law for the Cd release, derived from the CFD thermal analysis of the combusting particle, is proposed. The simulation results are compared with experimental data obtained in a lab-scale fluidized bed incinerator reported in literature, and with the predicted values from a particulate non-isothermal model, formerly developed by the authors. The comparison shows that the proposed CFD model represents very well the evolution of the HM release for the considered range of bed temperature.

© 2013 Elsevier B.V. All rights reserved.

## 1. Introduction

The problem of municipal solid waste disposal in landfill is becoming more and more a key issue as a consequence of the increasing amount of municipal solid waste produced worldwide and the environmental contamination associated with it. In this frame, fluidized bed incineration (FBI) appears as an effective waste management alternative to landfilling – less and less possible.

This high-temperature process can handle all types of waste: municipal solid waste, hazardous waste, medical waste, or sewage sludge by transforming them into more homogeneous

residues (flue gas, fly ash and bottom ash). When compared with landfilling, municipal solid waste (MSW) incineration presents several advantages such as reducing the solid waste volume by 80–90%, decreasing its reactivity by destroying (almost completely) organic compounds, biological threats (bacteria and viruses), and turning MSW into inert matter [1]. Furthermore, the heat produced by FBI method can be used to generate power and heat, achieving energy recovery. Additionally, the combustion temperature in FBI units rarely exceeds 1173 K, minimizing then, the formation of pollutants such as NO<sub>x</sub>, VOC and dioxins.

Despite these advantages, there is a great environmental and regulatory concern with respect to the metal emissions from waste incineration plants and to their toxicity [2]. Metal species contained in the waste are not destroyed during incineration; instead they may concentrate in the solid residues (bottom ash and fly

\* Corresponding author. Tel.: +33 4 6830 7757; fax: +33 4 6830 2940.  
E-mail address: [Daniel.Gauthier@promes.cnrs.fr](mailto:Daniel.Gauthier@promes.cnrs.fr) (D. Gauthier).

## Nomenclature

$c_p$	specific heat capacity, J/kgK
$C$	molar concentration, kmol/m <sup>3</sup>
$d_{pore}$	pore diameter, m
$D$	diffusivity, m <sup>2</sup> /s
$e_p$	particle emissivity
$E_a$	activation energy, J/kmol
$I$	radiation intensity, J/m <sup>2</sup> s
$L_0$	particle length, m
$k$	thermal conductivity, W/mK
$k_0$	pre-exponential Arrhenius' factor
$K$	permeability, m <sup>2</sup>
$M_w$	molecular weight, kg/kmol
$P$	pressure, Pa
$q$	metal concentration in waste, mg/kg
$q_0$	initial metal concentration in waste, mg/kg
$q_f$	final metal concentration in waste, mg/kg
$Q_{rad}$	net radiative heat transfer rate, J/s
$r_i$	reaction rate, kg/m <sup>3</sup> s
$r_{pore}$	mean pore radius, m
$R$	universal gas constant
$R_0$	particle radius, m
$t$	time, s
$T$	temperature, K
$v$	gas velocity, m/s
$x$	metal dimensionless concentration in waste
$X$	solid component mass fraction
$S_v$	specific surface area, m <sup>2</sup> /m <sup>3</sup>
$Y_i$	gas species mass fraction
<b>Greek letters</b>	
$\alpha_i$	stoichiometric coefficients for municipal solid waste pyrolysis
$\beta_{abs}$	absorption coefficient, m <sup>-1</sup>
$B_{sca}$	scattering coefficient, m <sup>-1</sup>
$\gamma$	stoichiometric coefficient for carbon combustion
$\Delta H$	reaction enthalpy, J/kg
$\varepsilon$	porosity
$\mu$	gas viscosity, Pa s
$\rho$	density, kg/m <sup>3</sup>
$\sigma$	Stefan–Boltzmann constant ( $5.672 \times 10^{-8}$ W/m <sup>2</sup> K <sup>4</sup> )
$\tau$	particle tortuosity
<b>Subscripts</b>	
0	initial
b	bed
C	residual carbon
HM	heavy metal
g	gas
s	solid
eff	effective
K	Knudsen
pore	pore

ash), be emitted with the incinerator's fumes, or even exit through the stack as airborne aerosols. Additionally, the heavy metal concentration in MSW is relatively higher than that in other solid fuels such as biomass and coal, and HM concentrations do vary strongly in MSW themselves [3]. Therefore, incinerators must be well designed and operated so as to minimize the risk associated with metallic emissions. It is then necessary to be able to predict the evolution of metal speciation and partitioning during this thermal process.

### 1.1. Previous experimental and theoretical studies in heavy metal vaporization

Several authors have studied, both experimentally [2,4–7] and theoretically—by thermodynamic modeling – [3,8–10], the heavy metal release from various particles. The metal speciation can be predicted from the waste and the gas compositions, but the transient system cannot be predicted by thermodynamics calculations only. Thus, the HM evolution must be investigated by kinetic studies.

Ho et al. [11] carried out experiments to study the metal behavior during the thermal treatment of contaminated soil. Their model kinetics parameters were identified with respect to experimental results. Abanades et al. [12] studied the kinetics of HM vaporization from model wastes in a fluidized bed. Both organic and mineral model wastes were used to study the influence of operating conditions on the extent of HM release in fumes. Liu et al. [13] determined the rate laws of toxic metal release during thermal treatment of model wastes. A first-order rate was determined for a mineral matrix, and a second-order rate was determined for a model waste, of composition similar to that of real waste.

More recently, Asthana et al. [14] investigated the behavior of three HM during the combustion of a waste bed traveling on an incinerator grate. They took experimental vaporization kinetics reported by Falcoz et al. [15], and coupled these laws to a previously developed mathematical model of the combustion of a MSW bed.

In this context, two objectives are set in this work. The first aim is to present and validate a local CFD model for predicting HM vaporization in front of experimental data published by Falcoz et al. [15]. The second one is to compare this CFD approach results against those reported previously by Mazza et al. [16]. In the next two subsections, the main characteristics concerning the HM vaporization experiments performed by Falcoz et al. [15] and the local model developed by Mazza et al. [16] are briefly described, respectively.

#### 1.1.1. Previous experimental work: Falcoz et al.'s experiments [15]

These authors studied the kinetics of HM vaporization from so-called realistic artificial waste (RAW) pellets made from MSW, in a laboratory fluidized bed reactor. These synthetic pellets were made from real MSW, sand, glue and metallic salt, then pressed into cylinders and dried. The pellet physical properties along with the ultimate analysis are shown in Table 1.

The experimental setup involved a high temperature, electrically-heated fluidized bed reactor coupled to a customized inductively coupled plasma optical emission spectrometer (ICP-OES). Experiments were carried out with solid samples impregnated with Cd at 923, 953, 983, 1013, 1043, and 1073 K. Once at thermal steady state, a given mass of reactive metal-spiked particles was injected into the bed composed of sand where the concentration of the HM vaporized in the exhaust gas was measured online by the ICP-OES technique.

After that, the vaporization rate at the particle level was determined from the experimental concentration profile in the fluid bed outlet gas, by using the inverse method previously developed and validated by Abanades et al. [17]. Finally, a kinetic law for metal release from realistic artificial waste was identified and the kinetic parameters were determined thanks to experiments carried out at several temperatures.

#### 1.1.2. Mazza et al.'s non isothermal model [16]

Mazza et al. [16] developed a non-isothermal particulate model for fluid bed MSW incineration combining solid waste particle combustion and HM vaporization from the burning particles. The model combines an asymptotic-combustion model for carbonaceous-solid combustion and a shrinking-core model to describe the HM

**Table 1**  
Particle properties.

Property	$\varepsilon_0$	$L_0$ [m]	$R_0$ [m]	$r_{pore}$ [ $\mu\text{m}$ ]	$\rho_{app,0}$ [ $\text{kg}/\text{m}^3$ ]	
Value	0.65	$1.5 \times 10^{-2}$	$0.5 \times 10^{-2}$	100	614	
Ultimate analysis	C	H	O	N	S	Ash
Weight % (dry basis)	45.9	6.5	30.5	1.0	0.3	15.8

vaporization phenomenon. It is in fact an improved version of the local model formulated previously and dealing with isothermal particle [10]. This improvement was necessary because, although the maximum values of predicted HM vaporization rates fitted well experimental results, the theoretical plots of HM vaporization rate versus metal concentration in the waste particle (i.e. versus time) were not in good agreement with experimental data. The non-isothermal particulate model takes also into account pyrolysis, combustion of pyrolysis gases, combustion of solid carbon, and metal vaporization. The system was numerically solved in FORTRAN (Compaq Visual FORTRAN 6.6), and their results showed that conduction in particle strongly affects the transient vaporization rate. Good fits were obtained with both the HM vaporization-rate trends and the maximum rates for all bed temperatures.

## 1.2. Physicochemical phenomena taking place during MSW incineration

The MSW thermal conversion includes complex chemical and physical processes such as: moisture evaporation, devolatilization, volatiles combustion, char gasification and char combustion and, usually, heavy metal vaporization. The time required for each reaction depends on the fuel size, its properties, and temperature and combustion conditions. These processes may occur sequentially or simultaneously, depending on particle properties and reactor conditions. The phenomena related to the creation and emission of pollutants during MSW combustion ( $\text{NO}_x$ , dioxins and furans) are not considered since the maximum operative temperature achieved in this work is less than 1173 K and, below this temperature, these pollutants emissions do not form in significant amounts.

### 1.2.1. Drying

Due to the intense heat transfer, the solid waste particle temperature rises rapidly after entering the fluidized bed. When the temperature of 373 K is reached, an intense process of evaporation and drying begins.

### 1.2.2. Devolatilization (pyrolysis)

As soon as the moisture is evaporated, the particle temperature rises up to 473–573 K and the devolatilization process starts. During this stage, the organic matter is weakened. It decomposes into a volatile fraction and a residual solid (char) as temperature increases. Pyrolysis is a complex process that depends on many different variables. The fundamentals of the process are still not completely understood and it is experimentally difficult to quantify the volatile species produced during this stage. Additionally, the heterogeneous nature of MSW (since it is a mixture of several components) induces thermal decomposition at various temperature levels. Di Blasi [18] presented a complete review of the existing devolatilization models.

### 1.2.3. Homogeneous gas combustion

It is difficult to isolate the combustion time from the devolatilization time because the two processes overlap. The pyrolysis gas mixture contains reaction products that are mainly  $\text{H}_2$ ,  $\text{CH}_4$  and CO. The oxygen in the air may oxidize these species. Although this is a complex set of reactions (as reported by Barbé et al. [19]),

mechanisms are not included in details but simplified by the following relations:



### 1.2.4. Residual carbon combustion

During the combustion of a char particle, oxygen from the bulk stream is transported to the surface of the particle, where it reacts with carbon to produce  $\text{CO}_2$  and CO (oxidation). Nonetheless, depending on the conditions (such as low temperatures), oxygen may diffuse into the pores and oxidize the carbon on their inner walls.

The combustion of both porous and non-porous particles has been widely studied, since it occurs in several processes of interest such as coal, wood, biomass, sludge and waste combustion [20–28]. Williams et al. [29] summarized the fundamental processes of solid combustion such as heating up, devolatilization and heterogeneous oxidation, and they outlined several models for these stages for coal and biomass cases.

### 1.2.5. Char gasification

$\text{CO}_2$  and steam may react with residual carbon, thus influencing the combustion, especially in oxygen-depleted zones. The reactions are:



The gasification reaction of residual carbon (Eq. (4)) is threefold faster than the Boudouard reaction (Eq. (5)) [30]. Carbon may also react with  $\text{H}_2$  to produce methane; however, this reaction, which is 300 times slower than the Boudouard reaction, is not likely to occur [30].

### 1.2.6. Metal vaporization

Several transformations may occur to the HM when incinerating MSW, as described by Asthana et al. [14]. The HM may either:

- I. vaporize under a chemical form dictated by thermodynamics that may differ from its original form,
- II. transform into another, more stable solid species,
- III. remain unchanged, or
- IV. be released as the result of the thermal degradation of the organic matrix in which it was trapped.

This study deals only with the events that comprise vaporization –(I) and (IV)–. The heterogeneous process of HM vaporization can be expressed as:



Many factors influence the heavy metal partitioning during incineration. Their reaction kinetics, as well as their vaporization, is related to their physico-chemical properties. Some incineration conditions have been identified as important parameters strongly affecting the

HM behavior (for instance: operative temperature, chlorine content, moisture content, retention time or mixing conditions, etc.) [15].

## 2. Cfd modeling approach

Fig. 1 shows the zoomed view of the adopted geometry along with the boundary conditions (the computational domain is larger than the particle). The porous waste particle is a cylinder of radius  $R_0$  and height  $L_0$ . The direction of the inlet main flow – air – is perpendicular to the longitudinal axis of the particle. In order to avoid possible numerical complications, mainly gas backflow, the computational domain is set significantly larger.

The thermal boundary condition at the sidewall is established as the mean bed temperature reported in the experiments  $T_b$  with the emissivity of the dense phase of the bed. “Velocity inlet” boundary condition is used for the gas entering the computational with a value equal to the fluidizing velocity reported by Falcoz et al. [31]—thus not in minimum fluidization conditions—and the fluid bed mean temperature  $T_b$ . The initial temperature of all system components (gas and particle) is equal to the mean bed temperature. Furthermore, the initial velocity inside the particle is set as zero so as to let oxygen diffusion happen over time, meanwhile “pressure outlet” is set at the exit of the geometry. Finally, symmetry boundary condition is used to minimize computational time.

User-defined functions (UDFs) are programmed in C++ language and coupled to the software in order to simulate the heterogeneous processes of solid combustion and heavy metal vaporization. In addition, UDFs mass sources for each gas species participating in the residual carbon combustion, as well as UDFs for energy source due to heterogeneous combustion, viscous resistance, porosity change, absorption coefficient, effective diffusivities are also programmed.

### 2.1. Main assumptions

Modeling the combustion of a porous MSW particle with HM vaporization requires various assumptions and simplifications. They are as follows:

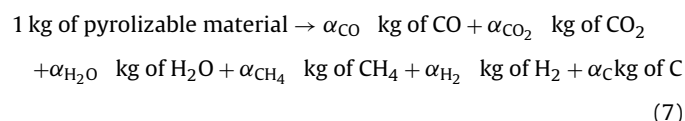
1. MSW pellets are cylindrical and homogeneous.
2. The main flow passing around the particle is laminar.
3. Local thermal equilibrium exists between the solid and gas phases in the particle, so internal temperatures and their gradients are the same for both the solid and gas.
4. Radiation heat transfer exists between the particle and the surrounding environment.
5. The particle structure is isotropic.
6. The porosity changes proportionally to the residual carbon conversion degree.
7. No ash remains around the particle after solid waste combustion (it is swept away by attrition).  
The assumptions concerning the Cd vaporization are:
8. Cd initial concentration is uniform.
9. Cd concentration in both the solid and the gaseous phases is negligible. Therefore, its contribution to the global mass and energy transport equations is not considered.
10. Cd vaporization begins in the residual carbon combustion stage. Some assumptions may be more likely to deviate, e.g. it is considered that the particle is isotropic while in reality it may present a non isotropic behavior. Also, it is assumed that the particle is homogeneous while in fact there is a considerable level of heterogeneity in its composition and pore distribution that could affect the applicability of the model. Nonetheless, if one wishes to consider the variations in structure, properties and concentrations within the particle, the model will

become too complex, with properties values difficult to obtain along with a high computational cost, thus losing one important aspect in modeling such as agility.

### 2.2. Modeling incineration stages

There is no particle drying phase because of the particle preparation procedure, which consists in impregnating the waste flakes with metallic salt solution, pressing into pellets and drying them in an oven, thus removing all the moisture content.

Ménard [32] treated pyrolysis by a “one step global mechanism” model, where the following stoichiometry relation was applied:

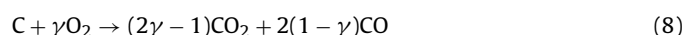


In the proposed CFD model, pyrolysis is supposed to be instantaneous with the coefficients given in Table 2, reported by Ménard [32]. Consequently, the gaseous species composition generated by this stage is set as the initial condition for CFD simulations. Also, the particle is supposed to be initially at the same temperature as the bed ( $T_s = T_b$ ).

Various authors consider that a fuel particle may shrink during pyrolysis [33–35], while others consider it enlarges [32,36,37]. Moreover, a few particles may present both behaviors through this thermal degradation [38]. In addition, pyrolysis is even considered as an endothermic reaction by some authors and as an exothermic reaction by others. Fortunately, it is negligible in front of the other thermal processes. On this basis, the pyrolysis enthalpy is assumed to be zero and the particle size is assumed to remain constant through this stage.

The homogeneous combustion is treated by a simplified approach that takes into account the main reactions only (Table 3). This can be done because of the uncertainty in quantifying the pyrolysis emissions and the slight importance of this step in the model [10]. Kinetic relationships and parameters are identical to those used by Ménard [32] (see Table 3). It is considered that these reactions may take place in the volume of the particle's pores as well as outside of it.

The residual carbon combustion model comprises an effective stoichiometry from the classical combustion reactions that lead to a CO–CO<sub>2</sub> mixture as the product, as can be seen in Eq. (8).



The primary CO/CO<sub>2</sub> ratio is very significant for the calculation of the particle temperature during combustion, because the lower the CO/CO<sub>2</sub> ratio, the higher the heat of reaction and the higher the temperature of the burning particle [26]. Arthur's law is used to calculate the ratio CO/CO<sub>2</sub> [32]:

$$\gamma = \frac{2 + f_c}{2(1 + f_c)}; f_c \frac{C_{\text{CO}}}{C_{\text{CO}_2}} = 1340 \exp\left(-\frac{63,500}{RT}\right) \quad (9)$$

The kinetic expression is given in Eq. (10).

$$r_c = k_{0,c} \cdot T e^{-(E_{ac}/RT)} C_{\text{O}_2} S_v (1 - \varepsilon) \quad (10)$$

It is a first order reaction, and its rate depends on the oxygen molar concentration in the gas and on the local cell temperature. The intrinsic pre-exponential factor and the activation energy are taken from Cooper and Hallett [21].

The gasification reactions of the residual carbon are neglected compared to its oxidation reaction because of the high temperature and of the oxidizing atmosphere existing in the bed environment.

For modeling the Cd release, the vaporization rate is calculated as a function of local conditions in the particle, especially



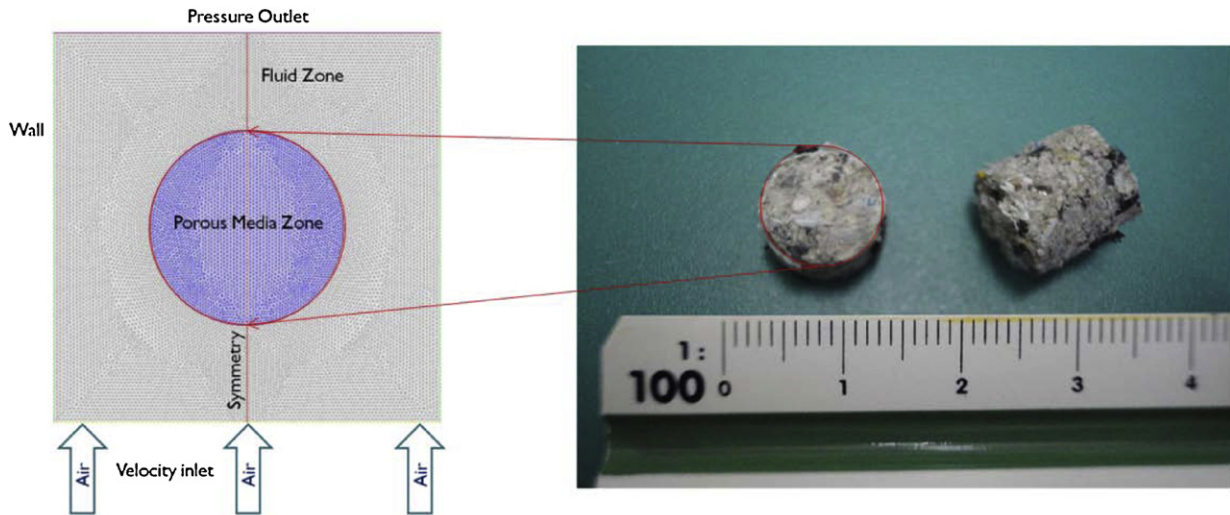


Fig. 1. Particle geometry and computational domain characteristics.

**Table 2**  
Stoichiometric coefficients for municipal solid waste pyrolysis.

Species	CO	CO <sub>2</sub>	H <sub>2</sub> O	CH <sub>4</sub>	H <sub>2</sub>	C
$\alpha_i$ [mass of $i$ /mass of pyrolyzable material]	0.378	0.133	0.111	0.178	0.022	0.177

temperature. The rate of vaporization  $r_{Cd}$ , is:

$$r_{Cd} = k_{0,Cd} e^{-(E_{a,Cd}/RT)} \left( \frac{10^6 X_{Cd} - q_f}{q_0 - q_f} \right)^n 10^{-6} \rho_{app,o} + \frac{r_c (X_{Cd} - 10^{-6} q_f)}{X_{c,0}} \quad (11)$$

The Arrhenius kinetic parameters and the reaction order were obtained from a thermal particle analysis by applying non-linear regression technique, which gave:

$$k_{0,Cd} = 3.65119 \cdot 10^{14} \text{ mg}/(\text{kg} \cdot \text{s})$$

$$E_{a,Cd} = 273753415.2 \text{ J/kmol}$$

$$n = 1.4$$

Two contributions to the Cd vaporization are considered. The first term in Eq. (11) relates the Cd vaporization rate to the local temperature level under an Arrhenius expression, and the second one relates the Cd release rate to the thermal degradation of the waste (in this case, char combustion).

### 2.3. Governing equations

The species mass transport equation for all gas phase components ( $i = \text{N}_2, \text{O}_2, \text{CO}, \text{CO}_2, \text{CH}_4, \text{H}_2, \text{H}_2\text{O}$ ) include the unsteady term, transport by convection and diffusion along with the source terms due to homogeneous and heterogeneous reactions as follows:

$$\frac{\partial(\varepsilon \rho_g Y_i)}{\partial t} + \nabla(\rho_g v Y_i) = \nabla(D_{\text{eff},i} \nabla Y_i) + r_i \quad (12)$$

**Table 3**  
Homogenous reactions and rate expressions.

$\hat{r}_i$	Reaction description	Reaction rate [kmol m <sup>-3</sup> s <sup>-1</sup> ]	$k_0$	Ea [J/kmol]	Ref
1	$\text{CO} + \frac{1}{2} \text{O}_2 \rightarrow \text{CO}_2$	$k_{0,1} e^{\frac{E_{a1}}{RT}} C_{\text{CO}}^{0.5} C_{\text{O}_2}^{0.5}$	$1.3 \times 10^{11}$	$1.255 \times 10^8$	[39]
2	$\text{H}_2 + \frac{1}{2} \text{O}_2 \rightarrow \text{H}_2\text{O}$	$k_{0,2} e^{\frac{E_{a2}}{RT}} C_{\text{H}_2} C_{\text{O}_2}$	$1.1 \times 10^{16}$	$7.5 \times 10^7$	[40]
3	$\text{CH}_4 + \frac{3}{2} \text{O}_2 \rightarrow \text{CO} + 2\text{H}_2\text{O}$	$k_{0,3} e^{\frac{E_{a3}}{RT}} C_{\text{CH}_4}^{0.7} C_{\text{O}_2}^{0.8}$	$5.0122 \times 10^{11}$	$2.008 \times 10^8$	[41]

where  $r_i$  is the net rate of production of species  $i$  by chemical reactions. CH<sub>4</sub>, H<sub>2</sub> and H<sub>2</sub>O species are involved only in homogeneous reactions. Then,  $r_i$  is expressed as:

$$r_i = M_{w,i} \sum_{j=1}^{j=N} \hat{r}_{i,j} \quad (13)$$

For the gas species involved in both the homogeneous reactions and the heterogeneous reaction of residual carbon combustion (O<sub>2</sub>, CO, CO<sub>2</sub>) the source term is given by:

$$r_{\text{O}_2} = -\gamma r_c \frac{M_{w,\text{O}_2}}{M_{w,c}} + M_{w,\text{O}_2} \sum_{j=1}^{j=N} \hat{r}_{\text{O}_2,j} \quad (14)$$

$$r_{\text{CO}_2} = (2\gamma - 1) r_c \frac{M_{w,\text{CO}_2}}{M_{w,c}} + M_{w,\text{CO}_2} \sum_{j=1}^{j=N} \hat{r}_{\text{CO}_2,j} \quad (15)$$

$$r_{\text{CO}} = 2(1 - \gamma) r_c \frac{M_{w,\text{CO}}}{M_{w,c}} + M_{w,\text{CO}} \sum_{j=1}^{j=N} \hat{r}_{\text{CO},j} \quad (16)$$

where the first member in the right hand side of Eqs. (14)–(16) represents the consumption (for O<sub>2</sub>) or the creation (for CO and CO<sub>2</sub>) rate due to residual carbon combustion, and the second member stands for homogeneous reactions.

For heterogeneous reactions of porous particles at high temperature, the overall rate of reaction becomes limited by diffusion in the pore structure of the particle, making the diffusion coefficient one of the main key parameters. For this reason, the influence of

both Knudsen (Eq. (17-a)) and molecular (Eq. (17-b)) diffusion is taken into account.

$$D_{k,i} = \frac{4}{3} \left( \frac{8RT}{\pi M_{w,i}} \right)^{1/2} K_0 \quad (17-a)$$

$$D_{AB} = \frac{0.001858 T^{1.5} M_{w,AB}^{1/2}}{P \sigma_{AB}^2 \Omega_D} \quad (17-b)$$

These two diffusivities are combined using the Bosanquet formula (valid particularly for equimolar counter diffusion) [42] so as to give an approximation value of the diffusion coefficients within the porous solid,  $D_{pore}$ , as shown in Eq. (17-c). Finally, Eq. (17-d) estimates the effective diffusivity taking into account the diffusion coefficient in the pores through the porosity of the solid,  $\varepsilon$ , and the tortuosity of the pores,  $\tau$ .

$$D_{pore} = \left( \frac{1}{D_{m,i}} + \frac{1}{D_{k,i}} \right)^{-1} \quad (17-c)$$

$$D_{eff,i} = \left( \frac{\varepsilon}{\tau} \right) D_{pore} \quad (17-d)$$

The overall gas-phase continuity equation results from the sum of these species transport equation and can be written:

$$\frac{\partial(\varepsilon \rho_g)}{\partial t} + \nabla(\rho_g v) = r_c \quad (18)$$

The classical momentum equation for porous media is used in this work, given by:

$$\frac{\partial(\varepsilon \rho_g v)}{\partial t} + \nabla(\rho_g v v) = -\nabla p + \nabla(\tau) + B_f - \frac{\mu}{K} v \quad (19)$$

where the value for permeability  $K$  is calculated by employing Darcy's law:

$$K = \frac{d_{pore}^2 \varepsilon^3}{150(1-\varepsilon)^2} \quad (20)$$

here,  $d_{pore}$  is taken as the local pore diameter inside the particle.

For the residual carbon, the conservation equation is:

$$\rho_{app,0} \frac{dX_c}{dt} = -r_c \quad (21)$$

It can be seen that the loss of residual carbon in the particle through time is due to heterogeneous combustion rate  $r_c$ .

Similarly, the mass balance for Cd in solid phase is given in Eq. (22). Eq. (23) represents the mass balance for vaporized Cadmium. It takes into account the unsteady term, mass transfer by convection and diffusion along with vaporization rate  $r_{Cd}$

$$\rho_{app,0} \frac{dX_{Cd}}{dt} = -r_{Cd} \quad (22)$$

$$\frac{\partial(\varepsilon \rho_g Y_{Cd})}{\partial t} + \nabla(\varepsilon \rho_g v Y_{Cd}) = \nabla(D_{eff,Cd} \nabla Y_{Cd}) + r_{Cd} \quad (23)$$

The Cd diffusion coefficient is taken by Asthana [43] which is calculated as a function of temperature from the kinetic gas theory:

$$D_{Cd,N_2} = 5.3974 \times 10^{-10} T^{1.7807} \quad (24)$$

The temperature profile in both the porous particle and the gas phase is obtained by solving the energy conservation equation. It comprises the unsteady term, heat transfer due to convection and conduction, the heat generated by the combustion of volatiles species, by residual carbon combustion and also takes into account radiation heat transfer expressed in the radiation source term  $S_{rad}$ :

$$\begin{aligned} &(\rho c_p)_{pm} \frac{\partial T}{\partial t} + (\rho c_p)_f v \nabla T \\ &= \nabla(k_{eff} \nabla T) + \sum_{j=1}^{j=N} r_j (-\Delta H_j) + r_c (-\Delta H_c) + S_{rad} \end{aligned} \quad (25)$$

with the specific heat capacity of the porous particle computed as:

$$(\rho c_p)_{pm} = \varepsilon(\rho c_p)_f + (1-\varepsilon)(\rho c_p)_s \quad (26)$$

and the effective thermal conductivity in the porous media,  $k_{eff}$ , expressed as the volume average of the fluid conductivity and the solid conductivity:

$$k_{eff} = \varepsilon k_f + (1-\varepsilon)k_s \quad (27)$$

Finally, the radiative transfer equation (RTE) for an absorbing, emitting, and scattering medium at position  $\vec{r}$  in the direction  $\vec{s}$  is:

$$\begin{aligned} &\frac{dI(\vec{r}, \vec{s})}{ds} + (\beta_{abs} + \beta_{sca}) I(\vec{r}, \vec{s}) \\ &= +\beta_{abs} n^2 \frac{\sigma T^4}{\pi} + \frac{\beta_{sca}}{4\pi} \int_0^{4\pi} I(\vec{r}, \vec{s}') \Phi(\vec{r}, \vec{s}') d\Omega' \end{aligned} \quad (28)$$

with the absorption coefficient  $\beta_{abs}$  given by:

$$\beta_{abs} = 1.5 \frac{(1-\varepsilon)e_p}{d_{pore}} \quad (29)$$

For each cell, the radiative source term  $S_{rad}$  is calculated as follows:

$$S_{rad} = -\nabla Q_{rad} = -4n^2 \beta_{abs} \sigma T^4 + \beta_{abs} G \quad (30)$$

with the incident radiation  $G$  represented in Eq. (31).

$$G = \int_{4\pi} I \vec{s} \cdot \vec{n} d\Omega \quad (31)$$

## 2.4. Numerical solution

The governing equations presented in the previous section are solved in 2-D using the CFD software FLUENT 12.1.4, which uses the finite volume discretization method. Although it is a 2D simulation, the dimension in the Z-axis is set as the particle's length in order to account for its volume [44]. The software solves numerically the momentum equation, the species mass transport equation, the local energy equation and the radiation heat transfer equation in the fluid as well as in the porous particle. An extensive set of UDFs subroutines was programmed and complemented to the code so as to represent residual carbon combustion and heavy metal vaporization.

The "pressure-based method" was applied to solve the momentum equation due to the low gas velocity. Additionally, second order discretization scheme was used for all scalars in order to obtain more accurate results. Moreover, it should be pointed out that the system is STIFF. The appropriate under-relaxation factors were set to avoid possible instabilities in the solution, thus reaching convergence in a lower number of iterations. The RTE was solved using the discrete ordinates method (DOM). The pixelation and angular discretization required by DOM in the frame of FLUENT are established at  $2 \times 2$ . Finally, the simulations were carried out in transient state, with a step size of 0.1 s and 40 iterations per time step.

## 3. Results and discussion

The Cd evolution during a typical MSW incineration process was calculated applying the proposed model, which uses commercial CFD code FLUENT 12.1.4 as the basic modeling platform to simulate hydrodynamics, momentum transport and homogenous combustion. In addition, all phenomena related to heterogeneous carbon combustion and heavy metal vaporization were simulated by self developed UDFs. The results of the CFD model are shown hereafter.

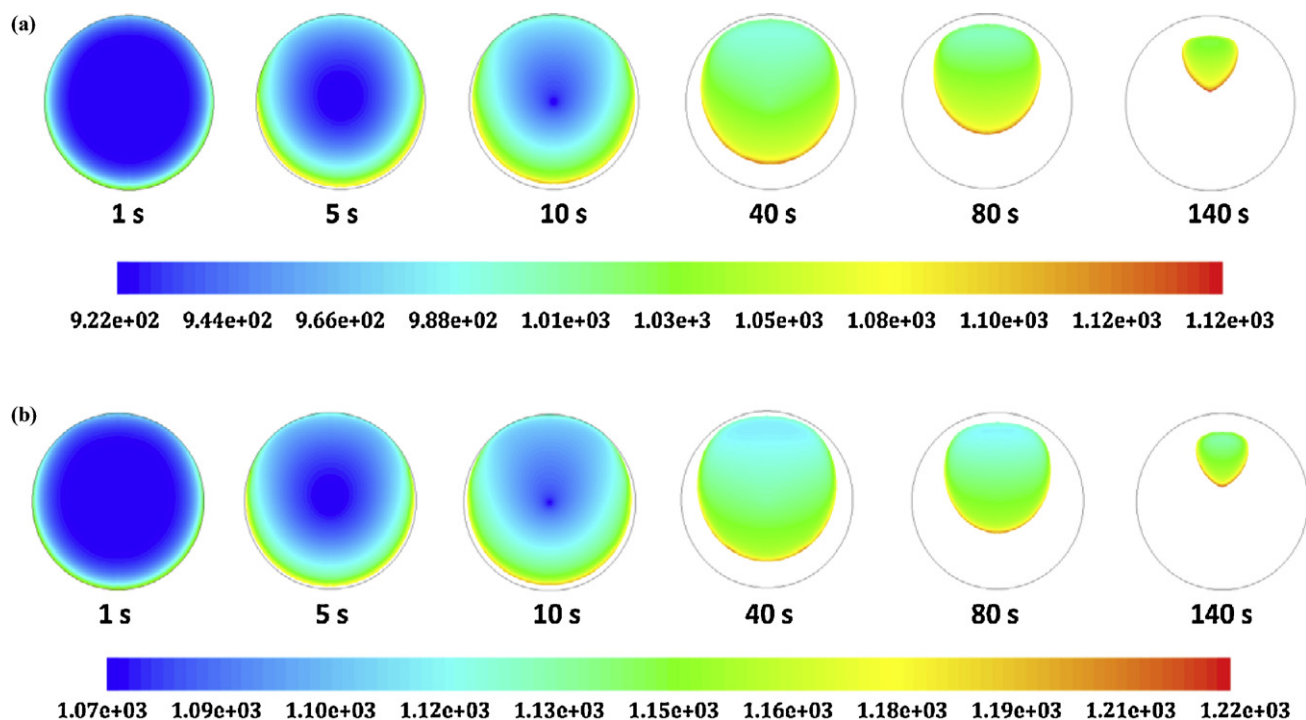


Fig. 2. Transient particle temperature profile at 923 K (a) and 1073 K (b).

### 3.1. Particle combustion and non-isothermal effects

Fig. 2 illustrates the temperature gradients inside the particle along with the decrement of the particle size at different simulation times for the limits of the temperature range studied (923 and 1073 K). Logically, the higher the temperature, the faster the waste particle shrinks. Results show that the time to completely burn the particle out at 923 and 1073 K are slightly different (174 s vs 170 s). This comes from the diffusion control of both processes, thus provoking the non-catalytic heterogeneous reaction at the particle surface. These results are in agreement with the observations stated in [22] and [26].

The model's prediction for the non-isothermal behavior inside the particle agrees qualitatively with the experimental and theoretical remarks found in bibliography [25,26]. Fig. 2 shows a wide temperature gradient, typical during combustion of large

biomass particle. In addition, it indicates that, logically, the highest level of temperature is found at the particle's bottom part surface: it corresponds to the zone where the higher combustion rates occur.

### 3.2. Influence of temperature on Cd vaporization

Fig. 3 plots the Cd vaporization rate versus time, for all operative bed temperatures analyzed. It can be appreciated that the model represents well the strong influence of temperature on the Cd vaporization dynamics. As expected, the higher the temperature, the higher the vaporization rate and the higher the Cd release (indicated by the area under the curve). The predicted metal vaporization rate is very high initially, and then it slows down during waste incineration, in accordance with experimental data. The maximum rates are also well calculated, except for the case

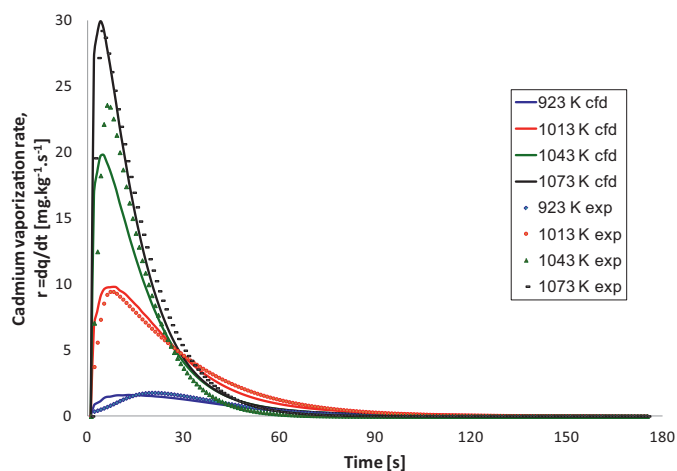


Fig. 3. Comparison between Cd vaporization rate temporal profile by CFD model and experimental results.

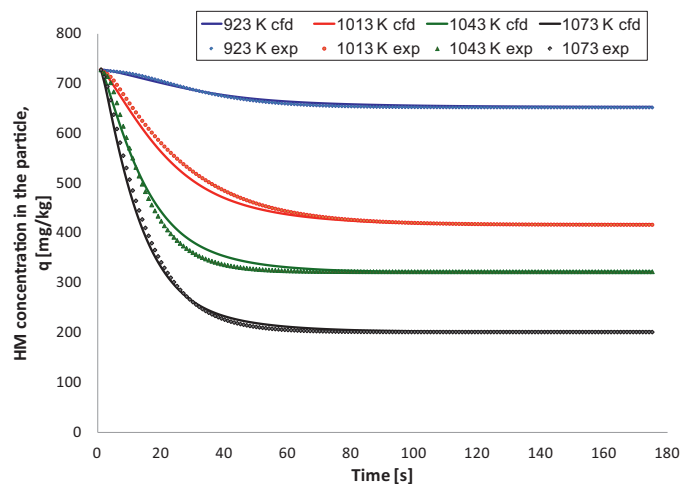


Fig. 4. Comparison between the predicted (CFD model) and the experimental Cd concentration profiles in the solid phase, for temperature range 923–1073 K.

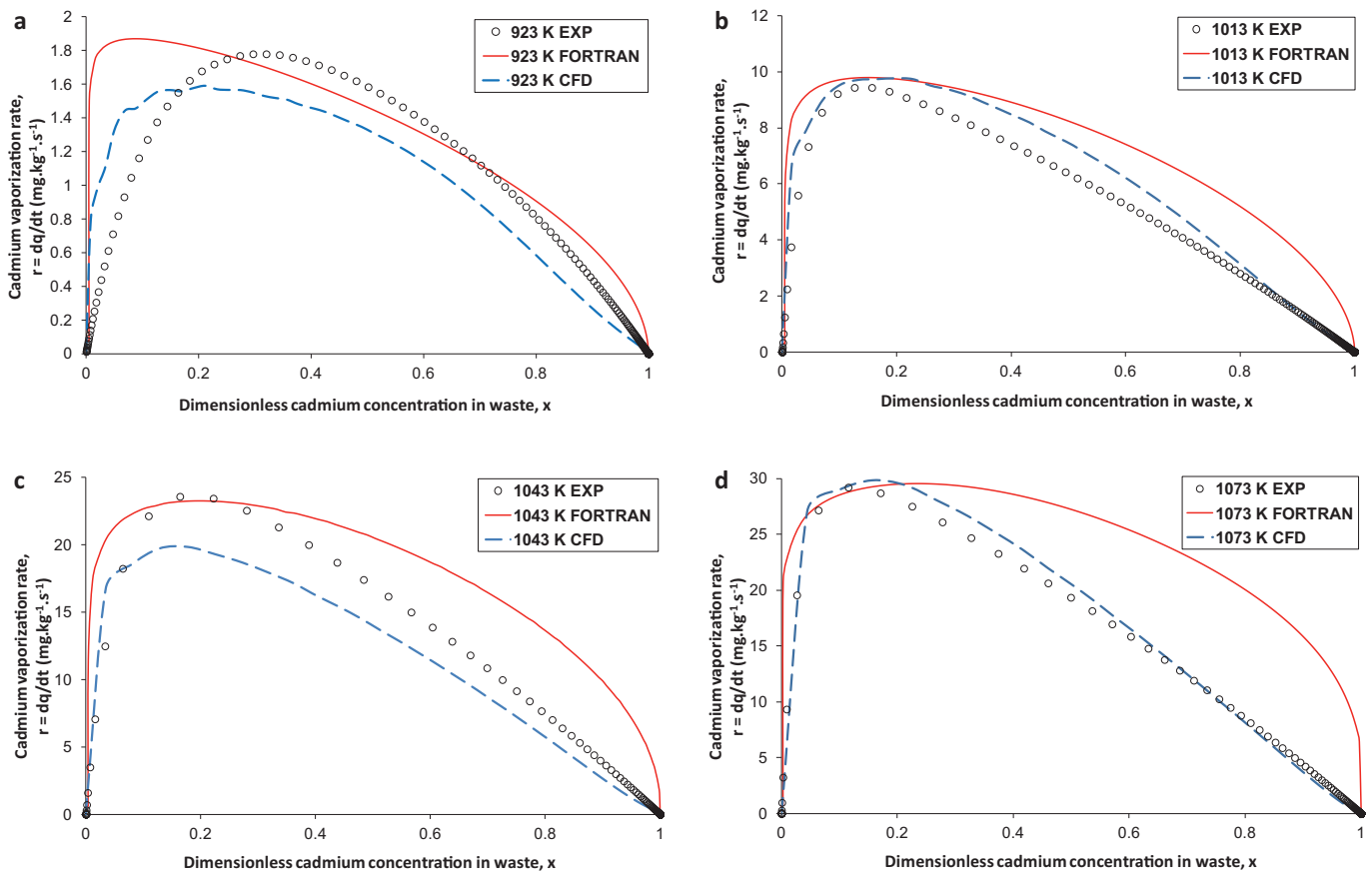


Fig. 5. Comparison between the experimental values, and both CFD and FORTRAN models' predictions: Cadmium,  $T = 923$  K (a),  $1013$  K (b),  $1043$  K (c) and  $1073$  K (d).

where  $T_b = 1043$  K where the model under-predicts the maximum rate value. Nonetheless, the overall behaviors for all experimental cases are very well represented. Additionally, the temperature influence on Cd vaporization rate is coherent and in agreement with the proposed Arrhenius law.

Fig. 4 compares, for different temperatures, the predicted temporal profiles of Cd concentration in the burning waste particle with experimental profiles. The comparison is very satisfactory, and results show how significantly temperature affects the metal vaporization: the higher the operative bed temperature  $T_b$ , the lower the Cd residual quantity in the particle,  $q_f$ .

Fig. 5 plots theoretical (from both FORTRAN and CFD models) and experimental cadmium vaporization rates versus the dimensionless metal concentration in waste ( $x$ ), at bed temperatures 923, 1013, 1043 and 1073 K, where

$$x = \frac{q_0 - q}{q_0 - q_f} \quad (32)$$

It can be seen that both models predict satisfactorily the experimental profile, and the CFD model represents better the initial stage of the Cd release for all bed temperatures. In addition, the shapes of the CFD theoretical curves are very similar to the experimental ones. Therefore, the CFD model fits better the experimental results, resulting more accurate than the FORTRAN model.

There are also some important features that support this CFD model as a better alternative, mainly the fact that it can predict the evolution of Cd behavior through time by means of a kinetic expression whereas the FORTRAN model does not reproduce this aspect since it is based on the existence of Cd equilibrium between the gaseous and solid phases. Additionally, in contrast with FORTRAN model, the CFD approach does not require the calculus of correlations for heat and mass transfer. FORTRAN model does not evaluate

the fluidynamic behavior through the momentum equation but adopts the simplification of perfect mix for the surrounding gas along with correlations to calculate velocities when needed. On the other hand, the new model developed by CFD solves the momentum equation allowing obtaining the velocity profile all over the computational domain.

In contrast, the main drawback of the CFD model is that it is high PC time consuming as a consequence of the high quality results demanded to the CFD model.

#### 4. Conclusions

A model for predicting the heavy metal vaporization during single particle MSW incineration in fluid bed has been developed with commercial CFD tool *ANSYS-FLUENT*, using the porous media approach along with an extensive array of UDFs developed to evaluate the fundamental aspects of kinetic, thermodynamic and structural characteristics of gas-solid reacting systems. This approach accounts for local variations of compositions and temperature occurring during the processes of instantaneous pyrolysis, homogeneous and residual carbon combustion.

Residual carbon combustion was modeled using an effective stoichiometry. Results suggest that, even for the lower temperature simulated, residual carbon oxidation is primarily diffusion-controlled. Moreover, model predictions showed that significant temperature gradients exist in large biomass particles during combustion.

A kinetic expression for Cd vaporization was obtained from CFD particle thermal analysis. It considers a contribution represented by an Arrhenius law and a second one due to residual carbon



combustion. Simulation results were compared very satisfactorily to experimental data obtained in a laboratory scale fluid bed incinerator, thus validating this methodology as a useful tool for better understanding HM vaporization from burning fuel particle.

An average description of the waste particle was adopted, with the HM uniformly distributed. However, despite the uncertainty on waste particle properties along with its heterogeneous structure, the present CFD model predicts very well the MSW evolution during its incineration.

## Acknowledgements

This study was developed in the frame of the CONICET-CNRS collaboration agreement. G. Mazza is a research member of CONICET (Argentina). The first author is especially grateful to the Argentine Agency of Scientific and Technological Promotion (ANPCyT) for granting his Ph.D. thesis.

## References

- [1] A. Jakob, S. Stucki, P. Kuhn, Evaporation of heavy metals during the heat treatment of municipal solid waste incinerator fly ash, *Environ. Sci. Technol.* 29 (9) (1995) 2429–2436.
- [2] S. Rio, C. Verwilghen, J. Ramarosan, A. Nzihou, P. Sharrock, Heavy metal vaporization and abatement during thermal treatment of modified wastes, *J. Hazard. Mater.* 148 (2007) 521–528.
- [3] L. Sørum, F.J. Frandsen, J.E. Hustad, On the fate of heavy metals in municipal solid waste combustion part I: devolatilisation of heavy metals on the grate, *Fuel* 82 (2003) 2273–2283.
- [4] L. Sun, S. Abanades, J.D. Lu, G. Flamant, D. Gauthier, Volatilization of heavy metals during incineration of municipal solid wastes, *J. Environ. Sci.* 16 (4) (2004) 635–639.
- [5] Y. Zhang, Y. Chena, A. Menga, Q. Li, H. Cheng, Experimental and thermodynamic investigation on transfer of cadmium influenced by sulfur and chlorine during municipal solid waste (MSW) incineration, *J. Hazard. Mater.* 153 (2008) 309–319.
- [6] H. Zhang, P.J. He, L.M. Shao, Fate of heavy metals during municipal solid waste incineration in Shanghai, *J. Hazard. Mater.* 156 (2008) 365–373.
- [7] S. Abanades, Comportement des métaux lourds dans le procédé d'incinération des déchets ménagers, Ph.D. Thesis, Université de Perpignan, Perpignan, 2001.
- [8] H. Zhou, S. Abanades, G. Flamant, D. Gauthier, J. Lu, Simulation of heavy metal vaporization dynamics in a fluidized bed, *Chem. Eng. Sci.* 57 (14) (2002) 2603–2614.
- [9] Y. Ménard, A. Asthana, F. Patisson, Ph. Sessiecq, D. Ablitzer, Thermodynamic study of heavy metals behavior during municipal waste incineration, *Process Saf. Environ. Prot.* 84 (B4) (2006) 290–296.
- [10] G. Mazza, Q. Falcoz, D. Gauthier, G. Flamant, A particulate model of solid waste incineration in a fluidized bed combining combustion and heavy metal vaporization, *Combust. Flame* 156 (11) (2009) 2084–2092.
- [11] T.C. Ho, H.W. Chu, J.R. Hopper, Metal volatilization and separation during incineration, *Waste Manage.* 13 (5–7) (1993) 455–466.
- [12] S. Abanades, G. Flamant, D. Gauthier, Kinetics of heavy metal vaporization from model wastes in a fluidized bed, *Environ. Sci. Technol.* 36 (2002) 3879–3884.
- [13] J. Liu, S. Abanades, D. Gauthier, G. Flamant, C. Zheng, J. Lu, Determination of kinetic laws for toxic metals release during thermal treatment of model waste in a fluid-bed reactor, *Environ. Sci. Technol.* 39 (2005) 9331–9336.
- [14] A. Asthana, Q. Falcoz, P. Sessiecq, F. Patisson, Modeling kinetics of Cd, Pb, and Zn vaporization during municipal solid waste bed incineration, *Ind. Eng. Chem. Res.* 49 (2010) 7605–7609.
- [15] Q. Falcoz, D. Gauthier, S. Abanades, G. Flamant, F. Patisson, Kinetic rate laws of Cd, Pb, and Zn vaporization during municipal solid waste incineration, *Environ. Sci. Technol.* 43 (2009) 2184–2189.
- [16] G. Mazza, Q. Falcoz, J. Soria, D. Gauthier, G. Flamant, Nonisothermal particle modeling of municipal solid waste combustion with heavy metal vaporization, *Combust. Flame* 157 (12) (2010) 2306–2317.
- [17] S. Abanades, G. Flamant, D. Gauthier, S. Tomas, L. Huang, Development of an inverse method to identify the kinetics of heavy metal release during waste incineration in fluidized bed, *J. Hazard. Mater.* A124 (2005) 19–26.
- [18] C. Di Blasi, Modeling chemical and physical processes of wood and biomass pyrolysis, *Prog. Energy Combust.* 34 (2008) 47–90.
- [19] P. Barbé, F. Battin-Leclerc, G.M. Côme, Experimental and modelling study of methane and ethane oxidation between 773 and 1573 K, *J. Chim. Phys.* 92 (9) (1995) 1666–1692.
- [20] S. Sriramulu, S. Sane, P. Agarwal, T. Mathews, Mathematical modelling of fluidized bed combustion – 1. Combustion of carbon in bubbling beds, *Fuel* 75 (12) (1996) 1351–1362.
- [21] P. Dacombe, M. Pourkashanian, A. Williams, L. Yap, Combustion-induced fragmentation behavior of isolated coal particles, *Fuel* 78 (15) (1999) 1847–1857.
- [22] J. Cooper, W.L.H. Hallett, A numerical model for packed-bed combustion of char particles, *Chem. Eng. Sci.* 55 (2000) 4451–4460.
- [23] C. Bruch, B. Peters, T. Nussbaumer, Modelling wood combustion under fixed bed conditions, *Fuel* 82 (2003) 729–738.
- [24] J. Porteiro, J.L. Míguez, E. Granada, J.C. Moran, Mathematical modelling of the combustion of a single wood particle, *Fuel Process. Technol.* 87 (2006) 169–175.
- [25] G. Canò, P. Salatino, F. Scala, Modelling fluidized bed combustion of a char particle with a coherent ash skeleton: application to granulated sewage sludge, *Fuel Process. Technol.* 88 (6) (2007) 577–584.
- [26] Y.B. Yang, V.N. Sharifi, J. Swithenbank, L. Ma, L.I. Darvell, J.M. Jones, M. Pourkashanian, A. Williams, Combustion of a single particle of biomass, *Energy Fuels* 22 (2008) 306–316.
- [27] V. Manovic, M. Komatina, S. Oka, Modeling the temperature in coal char particle during fluidized bed combustion, *Fuel* 87 (2008) 905–914.
- [28] H. Lu, W. Robert, G. Peirce, B. Ripa, L. Baxter, Comprehensive study of biomass particle combustion, *Energy Fuels* 22 (2008) 2826–2839.
- [29] A. Williams, M. Pourkashanian, J.M. Jones, The combustion of coal and some other solid fuels, *Proc. Combust. Inst.* 28 (2000) 2141–2162.
- [30] N.M. Laurendeau, Heterogeneous kinetics of coal char gasification and combustion, *Prog. Energy Combust. Sci.* 4 (1978) 221–270.
- [31] Q. Falcoz, Vaporisation des métaux lourds pendant l'incinération des déchets ménagers: cinétiques et processus de transfert, Ph.D. Thesis, Université de Perpignan, France, 2008.
- [32] Y. Ménard, Modélisation de l'incinération sur grille d'ordures ménagères et approche thermodynamique du comportement des métaux lourds, Ph.D. Thesis, Institut National Polytechnique de Lorraine, Nancy, 2003.
- [33] K.O. Davidsson, J.B.C. Pettersson, Birch wood particle shrinkage during rapid pyrolysis, *Fuel* 81 (3) (2002) 263–270.
- [34] A. Gomez-Barea, S. Nilsson, F. Vidal Barrero, M. Campoy, Devolatilization of wood and wastes in fluidized bed, *Fuel Process. Technol.* 91 (2010) 1624–1633.
- [35] C. Di Blasi, Heat, momentum and mass transport through a shrinking biomass particle exposed to thermal radiation, *Chem. Eng. Sci.* 51 (7) (1996) 1121–1132.
- [36] D. Dakića, G. van der Honing, M. Valk, Fragmentation and swelling of various coals during devolatilization in a fluidized bed, *Fuel* 68 (7) (1989) 911–916.
- [37] J. Yu, V. Strezov, J. Lucas, T. Wall, Swelling behavior of individual coal particles in the single particle reactor, *Fuel* 82 (2003) 1977–1987.
- [38] Z. Fu, Z. Guo, Z. Yuan, Z. Wang, Swelling and shrinkage behavior of raw and processed coals during pyrolysis, *Fuel* 86 (2007) 418–425.
- [39] J.B. Howard, G.C. Williams, D.H. Fine, Kinetics of carbon monoxide oxidation in post flame gases, in: 14th Symp. Int. on Combustion, The Comb. Inst., 1973, pp. 975–986.
- [40] P. Van Tiggelen, Oxydations et combustions, Technip Ed., Paris, 1968.
- [41] F.L. Dryer, I. Glassman, High temperature oxidation of CO and CH<sub>4</sub>, in: 14th Symp. Int. on Combustion, The Comb. Inst., 1973, pp. 987–1003.
- [42] G.F. Froment, K.B. Bischoff, Chemical reactor analysis and design, second ed., Wiley, New York, USA, 1979.
- [43] A. Asthana, Modélisation mathématique de la formation des NO<sub>x</sub> et de la volatilisation des métaux lourds lors de l'incinération sur grille d'ordures ménagères, Ph.D. Thesis, Institut National Polytechnique de Lorraine, Nancy, France, 2008.
- [44] ANSYS FLUENT, FLUENT User's guide 12.0, 2009.